International Journal of
Mathematics And its Applications
ISSN: 2347-1557

Int. J. Math. And Appl., **14(2)**(2026), 167–189
Available Online: http://ijmaa.in

Magnetohydrodynamic Flow of a Couple-Stress Fluid Through a Non-Homogeneous Porous Medium with Oscillatory Suction and a Heat Source/Sink

Anjali Kumari[1,*], Richa Tripathi[1]

[1]*Department of Mathematics, Gaya College, Gaya Ji (A Constituent Unit of Magadh University, Bodh gaya), Bihar, India*

Abstract

The present study investigates the heat and mass transfer characteristics of free convective flow of an incompressible, electrically conducting couple-stress fluid past a vertical porous plate embedded in a porous medium, in the presence of a uniform transverse magnetic field and internal heat source. The permeability of the porous medium and the suction velocity at the plate are assumed to vary periodically with time. The nonlinear governing partial differential equations describing the flow, thermal, and concentration fields are decomposed into steady and oscillatory components and subsequently reduced to a system of ordinary differential equations. An analytical solution is obtained using a regular perturbation technique. The effects of pertinent physical parameters on the velocity, temperature, and concentration distributions are examined and illustrated graphically, with particular emphasis on the influence of time-dependent suction and oscillatory permeability on the transport processes. The results demonstrate that periodic variations in permeability and suction significantly modify the flow structure as well as the thermal and solutal boundary layers of the couple-stress fluid. The results of this investigation are interesting for understanding transport phenomena in porous media with non-Newtonian fluids under periodically varying operating conditions.

Keywords: MHD flow; Porous medium; Permeability; Couple stress fluid; Mass and heat transfer; Source/sink.

2020 Mathematics Subject Classification: 76W05, 76S05, 76A05, 80A20, 35K57.

Nomenclature

C'	Species concentration	D	Molecular diffusivity
Gr	Grashof number for heat transfer	K'	Permeability of the medium
k	Thermal diffusivity	E	Non-dimensional Rotation parameter
H	Non-dimensional Heat source parameter	T	Non-dimensional temperature
t	Non-dimensional time	u	Non-dimensional velocity

*Corresponding author (anjalimishra89959@gmail.com)

v_0	Constant suction velocity	y	Non-dimensional distance along y-axis
ε	A small positive constant	β	Volumetric coefficient of expansion for heat transfer
β'	Volumetric coefficient of expansion with species concentration	$\nu = \frac{\mu}{\rho}$	Kinematic coefficient of viscosity
σ	Electrical conductivity	ω	Non-dimensional frequency of oscillation
C	Non-dimensional species concentration	Gc	Grashof number for mass transfer
g	Acceleration due to gravity	K_p	Non-dimensional Porosity parameter
M	Magnetic parameter	B_0	Magnetic field of uniform strength
Pr	Prandtl number	Sc	Schmidt number
T'	Temperature of the field	t'	Time
u'	Velocity component along x-axis	$v(t')$	Suction velocity
y'	Distance along y-axis	ρ	Density of the fluid
ω'	Frequency of oscillation	Ω	Rotation parameter
τ	Skin friction	ϕ	Non-dimensional couple stress parameter
η	Couple stress parameter	Nu	Nusselt Number
Sh	Sherwood Number	T	Non-dimensional temperature
Q	Heat Source parameter	$K_p^{'}$	Porosity parameter

1. Introduction

Magnetohydrodynamic (MHD) flow with simultaneous heat and mass transfer has attracted considerable attention due to its wide range of applications in science and engineering. Heat and mass transport from various geometries embedded in porous media arise in numerous engineering and geophysical processes, including drying of porous materials, thermal insulation systems, enhanced oil recovery, cooling of nuclear reactors, and underground energy transport. The couple-stress fluid theory represents a significant class of non-Newtonian fluid models that accounts for the influence of microstructural effects within the fluid. In contrast to classical Newtonian fluid theory, this model incorporates not only the symmetric part of the stress tensor but also additional couple stresses arising from the rotation of fluid microelements. Such microstructural contributions become particularly important in fluids containing polymeric additives, suspensions, or biological constituents. The model offers a more realistic representation of fluid behavior when the characteristic length scale of the microstructure is comparable to that of the flow domain. Owing to its relative mathematical tractability and physical relevance, the couple-stress fluid model has found wide applications in lubrication theory, magnetohydrodynamics (MHD), microfluidic devices, and biomedical engineering. The theoretical framework was systematically developed by V. K. Stokes in 1966 through the introduction of couple stresses in non-Newtonian fluids. Since its formulation, many investigations have been carried out to study the flow characteristics of couple-stress fluids in porous and nonporous media under different physical conditions.

A significant class of two-dimensional unsteady flow problems concerns the response of the

boundary layer to temporal fluctuations in the free-stream velocity about a mean state. Such phenomena are commonly encountered in buoyancy-driven flows in the atmosphere, oceans and other water bodies, as well as in quasi-solid geophysical systems such as the Earth's crust. In both natural processes and industrial operations, many transport mechanisms involve the simultaneous transfer of heat and mass, arising from the combined effects of thermal diffusion and species diffusion. Das [1] studied mass transfer effects on MHD flow and heat transfer over a vertical porous plate embedded in a porous medium with oscillatory suction in presence of a heat source. Dash [2] analyzed MHD Couette flow and heat transfer in a rotating channel taking into account the effects of viscous dissipation and heat source / sink highlighting the significance of rotation on the thermal characteristics. Kumar and Satyanarayana [3] studied mass transfer effects on unsteady MHD free convective Walters' memory fluid flow with constant suction and a heat sink. Prakash [4] examined heat transfer characteristics of MHD flow of a dusty viscoelastic (Walters' liquid model-B) stratified fluid in a porous medium under variable viscosity. Ravikumar [5] analysed combined heat and mass transfer effects on MHD flow of a viscous fluid through a non-homogeneous porous medium in the presence of a temperature-dependent heat source.

Hussaini [6] investigated unsteady MHD memory convective flow through a porous medium with variable suction and discussed its influence on velocity and temperature distributions. Mishra [7] analysed mass and heat transfer effects on MHD flow of a visco-elastic fluid through a porous medium with oscillatory suction and heat source. Mohanty [8] studied MHD flow of a viscoelastic fluid through a non-homogeneous porous medium with oscillatory suction and heat source/sink and presented numerical results for flow and heat transfer behaviour. Srinivasacharya and Kaladhar [9] investigated mixed convection in a couple stress fluid with Soret and Dufour effects, while in a later study they examined Soret and Dufour effects on mixed convection flow of a couple stress fluid in a non-Darcy porous medium with heat and mass fluxes [10].

Sharma [11] analysed MHD free convection radiative flow of a viscoelastic (Walters' liquid model-B) fluid in the presence of chemical reaction. Udayagiri [12] investigated unsteady MHD free convection flow characteristics of a viscoelastic fluid past a vertical porous plate and reported the influence of viscoelastic parameters on boundary-layer thickness. Ramaiah [13] examined chemical reaction and radiation absorption effects on MHD convective heat and mass transfer flow of a viscoelastic fluid past an oscillating porous plate with heat generation or absorption. Reddy [14] studied unsteady MHD free convection flow of a viscoelastic fluid past a vertical porous plate, focusing on the effects of magnetic and buoyancy parameters. Suneetha and Sailakumari [15] analysed heat and mass transfer characteristics of MHD free convective Rivlin–Ericksen fluid flow past a porous plate. Krishna and Chamkha [16] investigated MHD peristaltic rotating flow of a couple stress fluid through a porous medium with wall and slip effects. Krishna and Jyothi [17] analysed heat and mass transfer characteristics of MHD rotating flow of a viscoelastic fluid through a porous medium with time-dependent oscillatory permeability. Rajakumar [18] studied the influence of Dufour and thermal

radiation effects on unsteady MHD Walters' liquid model-B flow past an impulsively started infinite vertical plate embedded in a porous medium, incorporating chemical reaction, Hall and ion-slip currents. Poddar [19] presented steady-state solutions for MHD heat and mass transfer flow over a semi-infinite vertical plate in a rotating porous medium. Naveed [20] analysed heat transfer characteristics in hydromagnetic flow of a couple stress fluid and discussed the influence of magnetic parameters on thermal behaviour. Panya [21] examined MHD Darcy–Forchheimer slip flow in a porous medium with variable thermo-physical properties. Okuyade and Abbey [22] investigated transient MHD fluid flow past a moving vertical surface in a velocity slip regime and analysed the effects of slip and magnetic parameters. Mishra and Kumar [23] presented an analytical study of two-fluid flow in a porous inclined channel. Ahmad [24] developed a hydromagnetic slip flow model of fractional time and studied the influence of the fractional parameters on velocity fields Pegu [25] carried out a numerical investigation on viscoelastic fluid flow, focusing on heat and mass transfer characteristics.

The present study aims to investigate the effects of variable permeability and oscillatory suction velocity on free convective mass transfer flow of a couple-stress fluid past an infinite vertical porous plate embedded in a porous medium, under the influence of a uniform transverse magnetic field and a heat source/sink.

2. Mathematical Formulation

The present study investigates the oscillatory flow of an incompressible, electrically conducting, unsteady free convective couple-stress fluid past an infinite vertical porous plate embedded in a porous medium. The system is subjected to time-dependent oscillatory suction and variable permeability in the presence of a uniform transverse magnetic field. A Cartesian coordinate system is adopted such that the x'- axis is aligned along the plate in the direction of the flow, while the y'- axis is taken normal to the plate. Both the fluid and the plate are assumed to undergo rigid body rotation about the y - axis with constant angular velocity. The magnetic Reynolds number is considered to be much less than unity; consequently, the induced magnetic field is negligible compared to the applied transverse magnetic field. Under these assumptions, the flow within the porous medium is primarily driven by the buoyancy forces arising from the temperature difference between the plate and the ambient fluid. It is further assumed that for $t' \leq 0$, both the plate and the fluid are at the same uniform temperature, and the species concentration in the fluid is sufficiently small such that the Soret and Dufour effects can be neglected. For $t' > 0$, the plate temperature is instantaneously raised to a constant value T'_w, and the species concentration at the plate is similarly elevated to a constant value C'_w.

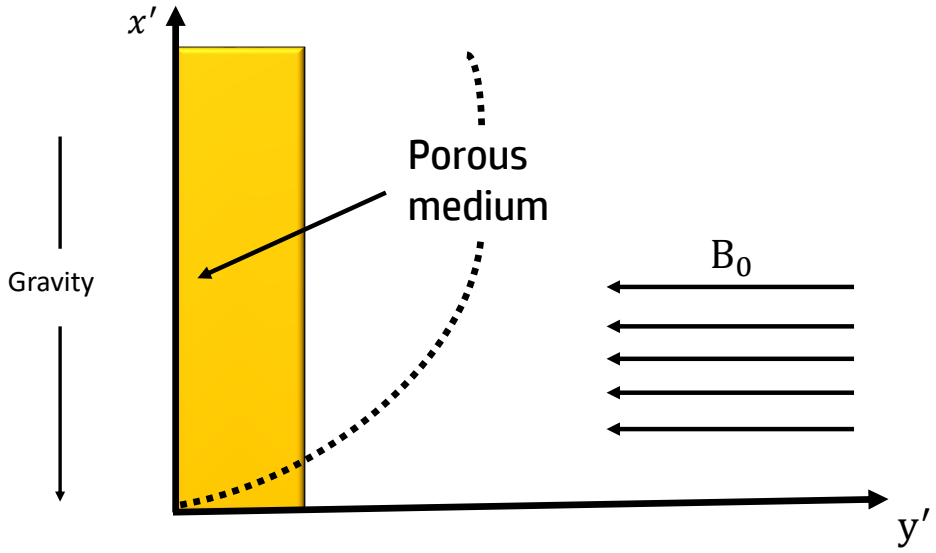

Figure 1: Flow geometry of the model.

The permeability of the porous medium and the suction velocity are assumed to be of the following form

$$K'(t') = K'_p\left(1 + \epsilon e^{i\omega' t'}\right) \tag{1}$$

$$v(t') = -v_0\left(1 + \epsilon e^{i\omega' t'}\right) \tag{2}$$

Here, $v_0 > 0$ and $\epsilon \ll 1$ are positive constants. Under the foregoing assumptions and invoking the Boussinesq approximation, the governing equations along with the corresponding boundary conditions are expressed as follows:

$$\frac{\partial u'}{\partial t'} + v\frac{\partial u'}{\partial y'} - 2\Omega v' = \frac{\mu}{\rho}\frac{\partial^2 u'}{\partial y'^2} + g\beta(T' - T_\infty) + g\beta^*(C' - C_\infty) - \frac{\sigma B_0^2}{\rho}u' - \frac{\mu u'}{\rho K'_p(1 + \varepsilon e^{i\omega' t'})} - \frac{\eta}{\rho}\frac{\partial^4 u'}{\partial y'^4} \tag{3}$$

$$\frac{\partial v'}{\partial t'} + v\frac{\partial v'}{\partial y'} + 2\Omega u' = \frac{\mu}{\rho}\frac{\partial^2 v'}{\partial y'^2} - \frac{\sigma B_0^2}{\rho}v' - \frac{\mu v'}{\rho K'_p(1 + \varepsilon e^{i\omega' t'})} - \frac{\eta}{\rho}\frac{\partial^4 v'}{\partial y'^4} \tag{4}$$

$$\frac{\partial T'}{\partial t'} + v\frac{\partial T'}{\partial y'} = K\frac{\partial^2 T'}{\partial y'^2} - Q(T' - T_\infty) \tag{5}$$

$$\frac{\partial C'}{\partial t'} + v\frac{\partial C'}{\partial y'} = D\frac{\partial^2 C'}{\partial y'^2} \tag{6}$$

Now Boundary conditions are

$$\left.\begin{aligned} u' = 0, v' = 0, T' = T_w + \epsilon(T_w - T_\infty)e^{i\omega' t'}, C' = C_w + \epsilon(C_w - C_\infty)e^{i\omega' t'}, \frac{\partial^2 u'}{\partial y'^2} = 0 \quad \text{at } y = 0 \\ u' \to 0, \quad v' \to 0, \quad T' \to T_\infty, \quad C' \to C_\infty, \quad \frac{\partial^2 u'}{\partial y'^2} \to 0 \quad \text{as } y \to \infty \end{aligned}\right\} \tag{7}$$

3. Non - Dimensionalization of Flow Quantities

To render the governing equations and the corresponding boundary conditions dimensionless, the following nondimensional variables and parameters are introduced:

$$\left.\begin{aligned} &y = \frac{v_0 y' \rho}{\mu}, \qquad t = \frac{v_0^2 t' \rho}{\mu}, \qquad \omega = \frac{\omega' \mu}{\rho v_0^2}, \qquad q' = \frac{q}{v_0}, \qquad u = \frac{u'}{v_0}, \\ &T = \frac{T' - T_\infty}{T_w - T_\infty}, \qquad E = \frac{\mu \Omega}{\rho v_0}, \qquad C = \frac{C' - C_\infty}{C_w - C_\infty}, \qquad \phi = \frac{\eta v_0^2 \rho^2}{\mu^3}, \\ &H = \frac{\mu Q}{\rho v_0^2}, \qquad K_p = \frac{v_0^2 K_p' \rho^2}{\mu^2}, \qquad M^2 = \frac{\sigma B_0^2 \mu}{\rho^2 v_0^2}, \qquad P_r = \frac{\mu}{\rho k'}, \\ &G_r = \frac{\mu g \beta (T_w - T_\infty)}{\rho v_0^3}, \qquad G_c = \frac{\mu g \beta' (C_w - C_\infty)}{\rho v_0^3}, \qquad S_c = \frac{\mu}{\rho D} \end{aligned}\right\} \tag{8}$$

The equations 3, 4, 5, 6 and 7 reduce to the following non-dimensional form:

$$\frac{\partial u}{\partial t} - (1 + \varepsilon e^{i\omega t}) \frac{\partial u}{\partial y} - 2Ev = \frac{\partial^2 u}{\partial y^2} + G_r\, T + G_c\, C - \frac{u}{K_p(1 + \varepsilon e^{i\omega t})} - M^2 u - \phi \frac{\partial^4 u}{\partial y^4} \Bigg\} \tag{9}$$

$$\frac{\partial v}{\partial t} - (1 + \varepsilon e^{i\omega t}) \frac{\partial v}{\partial y} + 2Eu = \frac{\partial^2 v}{\partial y^2} - \frac{v}{K_p(1 + \varepsilon e^{i\omega t})} - M^2 v - \phi \frac{\partial^4 v}{\partial y^4} \Bigg\} \tag{10}$$

$$\frac{\partial T}{\partial t} - (1 + \varepsilon e^{i\omega t}) \frac{\partial T}{\partial y} = \frac{1}{P_r} \frac{\partial^2 T}{\partial y^2} - HT \Bigg\} \tag{11}$$

$$\frac{\partial C}{\partial t} - (1 + \varepsilon e^{i\omega t}) \frac{\partial C}{\partial y} = \frac{1}{S_c} \frac{\partial^2 C}{\partial y^2} \Bigg\} \tag{12}$$

Assuming, $u(y,t) + iv(y,t) = q(y,t)$ then the momentum equations 9 and 10 becomes

$$\frac{\partial q}{\partial t} - (1 + \varepsilon e^{i\omega t}) \frac{\partial q}{\partial y} - 2Ei\, q = \frac{\partial^2 q}{\partial y^2} - \frac{q}{K_p(1 + \varepsilon e^{i\omega t})} - M^2 q - \phi \frac{\partial^4 q}{\partial y^4} + G_r\, T + G_c C \Bigg\} \tag{13}$$

The corresponding boundary conditions are -

$$\left.\begin{aligned} &q = 0, \quad T = 1 + \varepsilon e^{i\omega t}, \quad C = 1 + \varepsilon e^{i\omega t}, \quad \frac{\partial^2 q}{\partial y^2} = 0 && \text{at } y = 0 \\ &q \to 0, \quad T \to 0, \quad C \to 0, \quad \frac{\partial^2 q}{\partial y^2} \to 0 && \text{as } y \to \infty \end{aligned}\right\} \tag{14}$$

4. Method of Solution

In view of the periodic suction and the oscillatory temperature and concentration prescribed at the plate, the velocity, temperature, and concentration fields in the vicinity of the plate are assumed to be periodic in nature.

$$q(y,t) = q_0(y) + \epsilon q_1(y) e^{i\omega t} + O(\epsilon^2) \tag{15}$$

$$T(y,t) = T_0(y) + \epsilon T_1(y) e^{i\omega t} + O(\epsilon^2) \tag{16}$$

$$C(y,t) = C_0(y) + \epsilon C_1(y) e^{i\omega t} + O(\epsilon^2) \tag{17}$$

The aforementioned solution methodology has been employed by Mishra [7], Das [1], and Gireesh Kumar and Satyanarayana [3] for the analysis of periodically fluctuating flow problems. Upon substituting Equations (15)–(17) into Equations (11)–(13) and equating the coefficients of the non-harmonic terms (corresponding to ϵ^0) and the harmonic terms (corresponding to ϵ), the following set of equations is obtained:

$$-\phi \frac{d^4 q_0}{dy^4} + \frac{d^2 q_0}{dy^2} + \frac{dq_0}{dy} - \left(M^2 + 2iE + \frac{1}{K_p}\right) q_0 = -G_r T_0 - G_c C_0 \tag{18}$$

$$-\phi \frac{d^4 q_1}{dy^4} + \frac{d^2 q_1}{dy^2} - \left(M^2 + 2iE + \frac{1}{K_p} + i\omega\right) q_1 = -\frac{dq_0}{dy} - G_r T_1 - G_c C_1 - \frac{u_0}{K_p} \tag{19}$$

$$\frac{d^2 T_0}{dy^2} + P_r \frac{dT_0}{dy} - P_r H T_0 = 0 \tag{20}$$

$$\frac{d^2 T_1}{dy^2} + P_r \frac{dT_1}{dy} - P_r (H + i\omega) T_1 = -P_r \frac{dT_0}{dy} \tag{21}$$

$$\frac{d^2 C_0}{dy^2} + S_c \frac{dC_0}{dy} = 0 \tag{22}$$

$$\frac{d^2 C_1}{dy^2} + S_c \frac{dC_1}{dy} - i\omega S_c C_1 = -S_c \frac{dC_0}{dy} \tag{23}$$

The boundary conditions now reduce to

$$\left.\begin{aligned} & q_0 = q_1 = 0, \quad T_0 = T_1 = 1, \quad C_0 = C_1 = 1 \qquad \text{at } y = 0 \\ & q_0 = q_1 \to 0, \quad T_0 = T_1 \to 0, \quad C_0 = C_1 \to 0 \qquad \text{as } y \to \infty \\ & \frac{d^2 q_0}{dy^2} = 0 \quad \& \quad \frac{d^2 q_1}{dy^2} = 0 \qquad \text{at } y = 0 \\ & \frac{d^2 q_0}{dy^2} \to 0 \quad \& \quad \frac{d^2 q_1}{dy^2} \to 0 \qquad \text{as } y \to \infty \end{aligned}\right\} \tag{24}$$

The numerical solutions of the differential Equations (18)–(23), together with the associated boundary conditions given in Equation (24), which govern the velocity $q(y,t)$, temperature $T(y,t)$, and concentration $C(y,t)$ fields, are obtained by employing a fourth-order perturbation technique.

4.1 Skin-friction Coefficient (τ)

The shear stress (skin friction) at the surface of the plate, represented in terms of its amplitude, is formulated as follows:

$$\tau = \left.\frac{\partial q_0}{\partial y}\right|_{y=0} + \varepsilon e^{i\omega t} \left.\frac{\partial q_1}{\partial z}\right|_{y=0} - \phi \left[\left.\frac{\partial^3 q_0}{\partial y^3}\right|_{y=0} + \varepsilon e^{i\omega t} \left.\frac{\partial^3 q_1}{\partial y^3}\right|_{y=0}\right]$$

4.2 Nusselt Number (Nu)

The rate of heat transfer (heat flux) at the plate, expressed in terms of its amplitude, is evaluated by the following expression:

$$Nu = -\left[\left.\frac{\partial T_0}{\partial y}\right|_{y=0} + \varepsilon e^{i\omega t}\left.\frac{\partial T_1}{\partial y}\right|_{y=0}\right]$$

4.3 Sherwood Number (Sh)

The mass transfer coefficient (Sherwood number) at the plate, represented in terms of its amplitude, is defined by the following expression:

$$Sh = -\left[\left.\frac{\partial C_0}{\partial y}\right|_{y=0} + \varepsilon e^{i\omega t}\left.\frac{\partial C_1}{\partial y}\right|_{y=0}\right]$$

5. Results and Discussion

The present study examines heat and mass transfer characteristics in the free convective flow of an incompressible, electrically conducting couple-stress fluid past a vertical non-homogeneous porous plate embedded in a porous medium. The analysis incorporates time-dependent oscillatory permeability and suction, a uniform transverse magnetic field, and the influence of a heat source/sink. The governing equations are solved using a multi-parameter perturbation technique to obtain approximate analytical solutions for the velocity, temperature, and concentration distributions. The flow behavior is governed by several non-dimensional parameters, namely the magnetic parameter M, porosity parameter K_p, Grashoff number for heat transfer G_r, Grashof number for mass transfer G_c, frequency of oscillation ω, Schmidt number S_c, Prandtl number P_r, heat source parameter H, couple-stress parameter ϕ, and rotation parameter E. The numerical results corresponding to various values of these governing parameters are presented graphically in Figures (2 - 9) and tabulated in Tables (1 - 12). For the numerical computations, the baseline values of the parameters are selected as $M = 3$, $\omega = 1$, $\phi = 2$, $K_p = 0.6$, $P_r = 0.5$, $G_c = 1$, $G_r = 1$, $S_c = 1.5$, $H = 1$, $\varepsilon = 1$, $t = 2$, and $E = 0.5$, except in those cases where a particular parameter is varied to examine its individual influence on the flow, thermal, and concentration fields. The effects of various governing parameters on the velocity $q(y,t)$, temperature $T(y,t)$, and concentration $C(y,t)$ distributions are illustrated in Figures 2 to 9. These figures collectively demonstrate the influence of different physical parameters on the transport characteristics of the flow field.

Figures 2 presents the variation of velocity with respect to the couple-stress parameter ϕ, magnetic parameter M, porosity parameter K_p, and heat source parameter H. It is observed that an increase in the couple-stress parameter ϕ leads to a reduction in fluid velocity, which may be attributed to the enhanced internal resistance generated by couple stresses. Similarly, increasing the magnetic

parameter M results in a decrease in velocity due to the action of the Lorentz force, which opposes the fluid motion. The velocity further decreases with increasing porosity parameter K_p, as higher porous resistance impedes the flow. A marginal decline in velocity is also noted with an increase in the heat source parameter H, reflecting its indirect influence on the momentum field through thermal–momentum coupling.

Figures 3 illustrates the effects of the thermal Grashof number G_r and oscillation frequency ω on the velocity profile. An increase in the positive Grashof number G_r enhances the fluid velocity due to the intensification of thermal buoyancy forces. For negative values of G_r, an increase in its magnitude modifies the velocity distribution and leads to an increase in velocity as buoyancy effects become more significant. These observations confirm the dominant role of thermal buoyancy forces in governing the flow behavior. Furthermore, an increase in the oscillation frequency ω reduces the velocity, indicating that higher oscillatory effects suppress the flow and diminish the peak velocity.

Figures 4 depicts the variation of velocity with respect to the Prandtl number P_r, Schmidt number S_c, mass Grashof number G_c, and rotation parameter E. It is found that increasing the Prandtl number P_r reduces the velocity, which can be attributed to the thinning of the momentum boundary layer associated with lower thermal diffusivity. Similarly, an increase in the Schmidt number S_c decreases the velocity due to reduced mass diffusivity. In contrast, the velocity increases with increasing mass Grashof number G_c, as stronger concentration-induced buoyancy forces accelerate the flow. The rotation parameter E significantly modifies the velocity distribution, indicating that rotational effects alter the overall flow structure and influence the peak velocity.

Figures 5 illustrates the influence of time and the small positive constant ε on the velocity profile. As time progresses, a slight modification in the velocity distribution is observed, accompanied by a marginal increase in the peak velocity, indicating the gradual development of the momentum boundary layer. A pronounced enhancement in velocity occurs with increasing values of ε, demonstrating that this parameter exerts a positive influence on the flow strength and contributes to the acceleration of the fluid motion.

Figures 6 presents the temperature distribution for different values of the heat source parameter H and oscillation frequency ω. Increasing positive values of H reduce the temperature throughout the boundary layer and decrease the thermal boundary layer thickness. In contrast, negative values of H produce oscillatory temperature profiles with higher peak temperatures, indicating intensified thermal fluctuations and a thickening of the thermal boundary layer. An increase in the oscillation frequency ω results in a slight reduction in temperature near the plate, reflecting suppressed thermal diffusion.

Figures 7 depicts the effects of the Prandtl number P_r and time t on the temperature field. An increase in P_r significantly decreases the temperature distribution and reduces the thermal boundary layer thickness due to lower thermal diffusivity. A gradual and marginal decline in temperature with increasing time suggests stabilization of the thermal boundary layer as the flow evolves. Figures 8 shows the variation of concentration with respect to the Schmidt number S_c. For negative values of

ε, the concentration decreases near the plate and increases away from it, indicating modified mass diffusion characteristics. Increasing positive values of S_c reduce the concentration distribution and thin the concentration boundary layer, demonstrating that higher Schmidt numbers suppress mass diffusivity within the flow.

Figures 9 illustrates the combined influence of the small positive constant ε, oscillation frequency ω, and time t on the concentration profile. An increase in ε slightly enhances the concentration near the plate, indicating a mild thickening of the concentration boundary layer. Higher oscillation frequencies marginally suppress mass diffusion and reduce the concentration near the plate. Increasing time leads to an enhancement of the concentration distribution and promotes the growth of the concentration boundary layer, reflecting the progressive diffusion of species into the fluid.

The numerical values of the shear stress at the plate corresponding to different governing parameters are presented in Tables 1 to 12. Table 1 shows the variation of shear stress with the magnetic parameter M for different phase angles ωt. It is observed that the shear stress decreases monotonically as M increases from 1 to 5 for all values of ωt. This reduction is attributed to the Lorentz force generated by the applied transverse magnetic field, which opposes the fluid motion and diminishes the velocity gradient at the plate.

Table 2 presents the effect of the couple-stress parameter ϕ on the shear stress at the plate. The results indicate that the shear stress decreases markedly as ϕ increases from 2 to 20 for all phase angles. This behavior suggests that enhanced couple-stress effects increase the internal resistance of the fluid, thereby reducing the wall shear stress.

Table 3 illustrates the variation of shear stress with the porosity parameter K_p. It is evident that increasing K_p from 0.1 to 0.5 results in an increase in shear stress for all values of ωt. This trend is attributed to the increased permeability of the porous medium, which reduces flow resistance and enhances the fluid motion near the plate, thereby increasing the velocity gradient at the wall. Table 4 demonstrates the influence of the heat source parameter H on the shear stress. The results reveal that shear stress decreases as H increases from 0.1 to 0.5 for all phase angles. This decline may be attributed to the additional thermal energy introduced into the fluid, which alters the coupled momentum and thermal fields and weakens the velocity gradient at the plate. Table 5 presents the variation of shear stress with the thermal Grashof number G_r for different values of ωt. It is observed that the shear stress increases steadily as G_r increases from 0.1 to 0.9 for all phase angles. This behavior is due to the strengthening of thermal buoyancy forces, which accelerate the fluid motion and consequently increase the velocity gradient at the plate. Table 6 shows the effect of the Prandtl number P_r on the shear stress for different phase angles ωt. It is observed that the shear stress decreases as P_r increases from 0.1 to 0.5 for all values of ωt. This reduction is attributed to the decrease in thermal diffusivity associated with higher Prandtl numbers, which weakens the thermal boundary layer and consequently reduces the velocity gradient at the plate. Table 7 illustrates the variation of shear stress with the Schmidt number S_c. The results indicate a gradual decline in shear stress as S_c increases from 1.3 to 1.7 for

all phase angles. Physically, higher Schmidt numbers correspond to lower mass diffusivity, which suppresses species diffusion and reduces the associated buoyancy-driven momentum near the wall, thereby decreasing the wall shear stress. The influence of the mass Grashof number G_c is presented in Table 8. It is evident that the shear stress increases steadily as G_c increases from 0.1 to 0.5 for all values of ωt. This enhancement is due to the intensification of solutal buoyancy forces, which accelerate the fluid and increase the velocity gradient at the plate. Table 9 examines the effect of the rotation parameter E on the shear stress. Variations of E from -0.1 to -0.9 produce only marginal changes in shear stress for all phase angles, indicating that rotational effects are relatively weak under the specified flow conditions. The variation of the Nusselt number Nu with the Prandtl number Pr is presented in Table 10 for different phase angles ωt. The results show that Nu increases consistently as Pr increases from 0.1 to 0.5 for all phase angles, demonstrating that higher Prandtl numbers enhance the rate of heat transfer at the plate. However, for a fixed value of Pr, the Nusselt number decreases as ωt increases from 0 to $3\pi/4$, reflecting the damping effect of oscillatory motion on heat transfer. Table 11 presents the variation of the Nusselt number with the heat source parameter H for $\omega t = 0$, $\pi/4$, $\pi/2$, and $3\pi/4$. It is observed that an increase in H from 0.1 to 0.5 leads to a corresponding increase in Nu at all phase angles, indicating that the heat source parameter enhances the heat transfer rate at the wall. Nevertheless, for a fixed value of H, Nu decreases as the phase angle ωt increases from 0 to $3\pi/4$.

Finally, Table 12 reports the variation of the Sherwood number S_h with the Schmidt number Sc for $\omega t = 0$, $\pi/4$, $\pi/2$, and $3\pi/4$. As Sc increases from 0.1 to 0.2, the Sherwood number increases uniformly at all phase angles, indicating enhanced mass transfer at the plate. For $Sc = 0$, the Sherwood number remains negligibly small over the entire range of ωt. In the case of negative Schmidt numbers ($Sc = -0.1$ and $Sc = -0.11$), S_h is extremely small at $\omega t = 0$ but increases progressively as ωt advances from 0 to $3\pi/4$. Overall, higher positive values of Sc promote stronger mass transfer at the plate, as reflected by the increase in the Sherwood number.

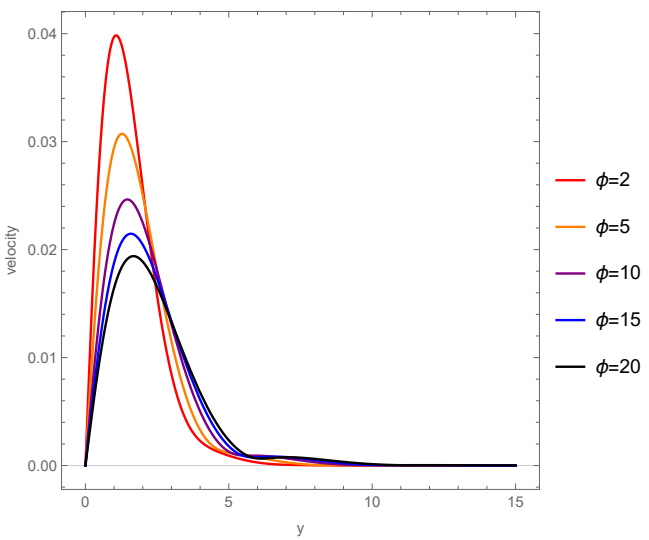

(a) Variation of $q(y,t)$ for (couple stress parameter ϕ).

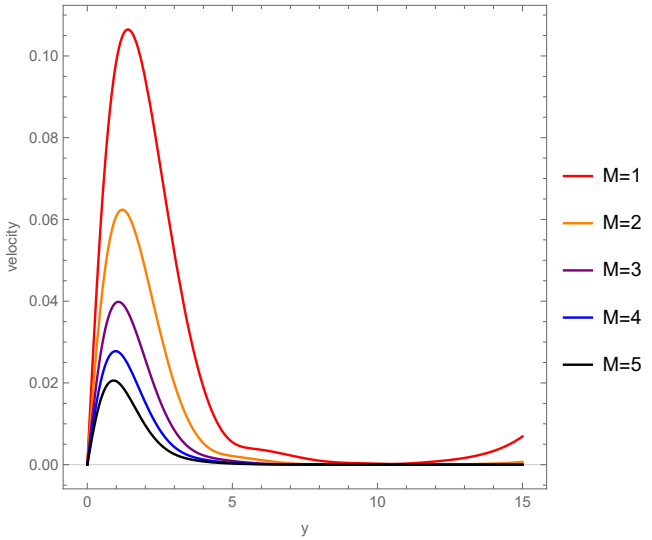

(b) Variation of $q(y,t)$ for (Magnetic parameter M).

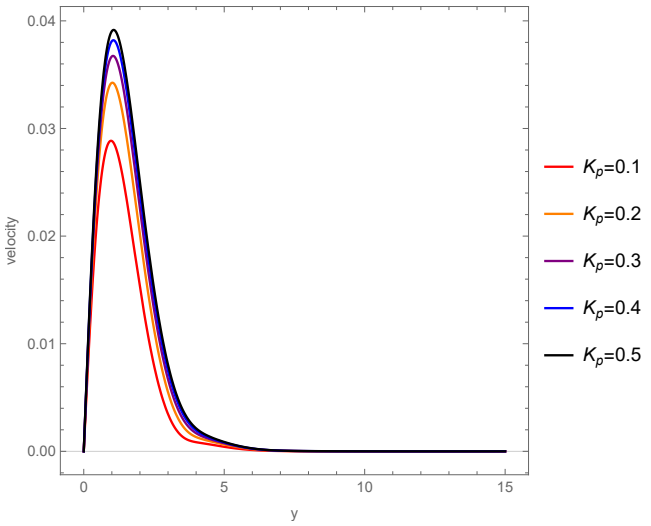

(c) Variation of $q(y,t)$ for (Porosity parameter K_p).

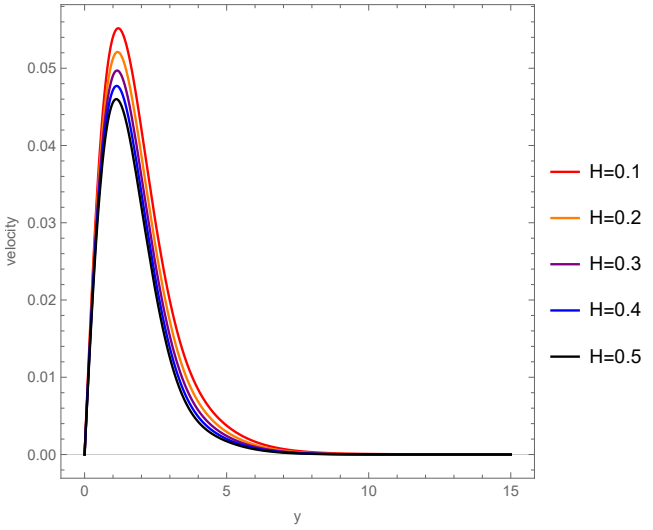

(d) Variation of $q(y,t)$ for (Heat Source parameter H).

Figure 2: Variation of velocity with different flow parameters

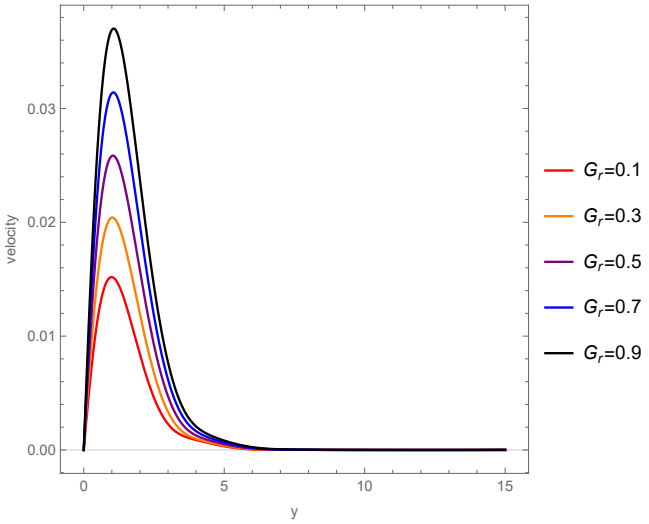

(a) Variation of $q(y,t)$ for (Grashof number for heat transfer G_r).

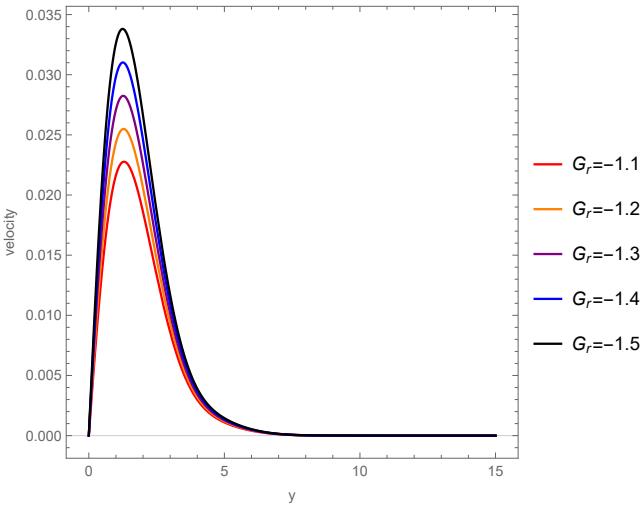

(b) Variation of $q(y,t)$ for (Grashof number for heat transfer G_r).

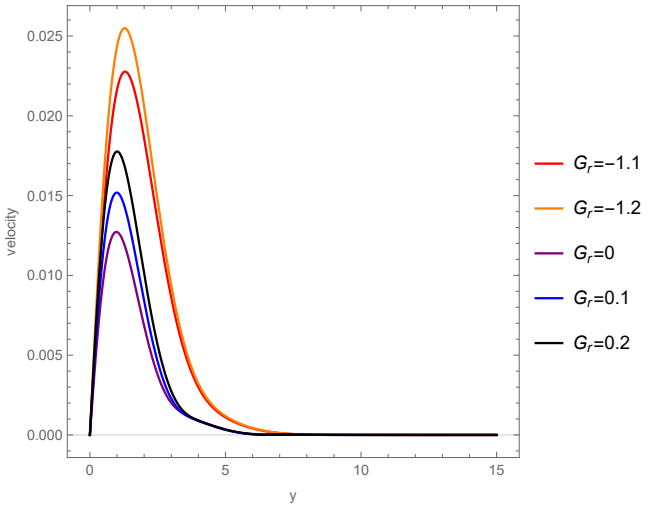

(c) Variation of $q(y,t)$ for (Grashof number for heat transfer G_r).

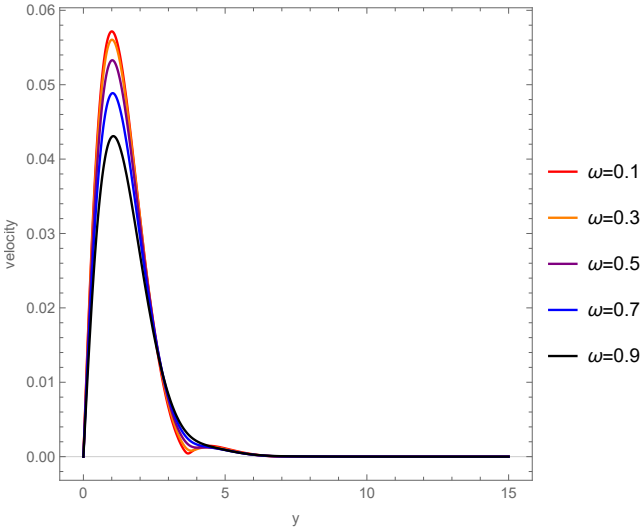

(d) Variation of $q(y,t)$ for (Frequency of oscillation ω).

Figure 3: Variation of velocity with different flow parameters

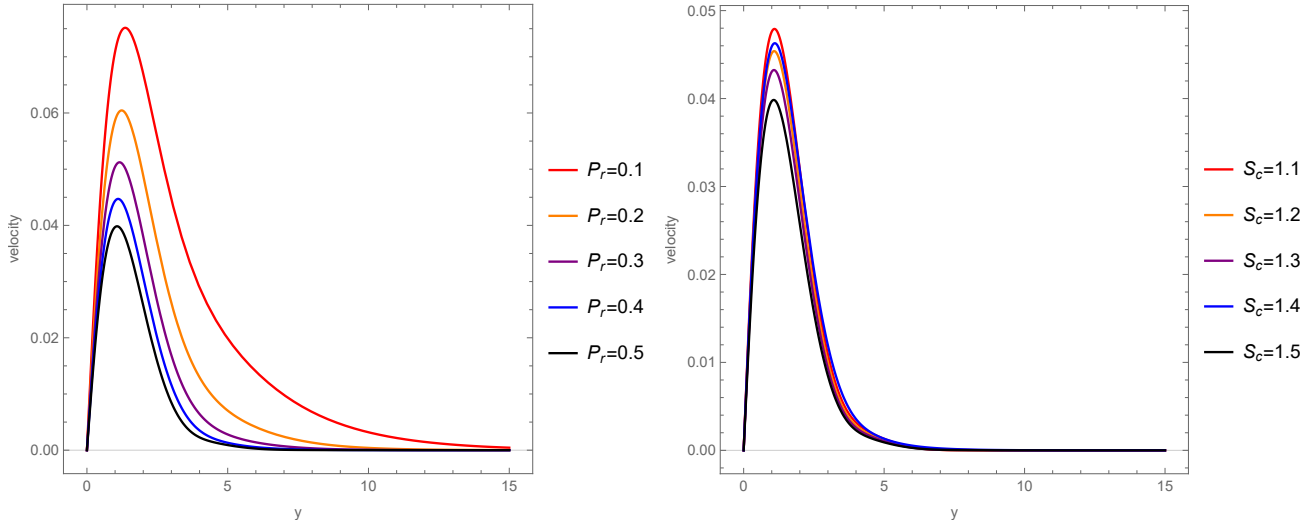

(a) Variation of $q(y,t)$ for (Prandtl number P_r).

(b) Variation of $q(y,t)$ for (Schmidt number S_c).

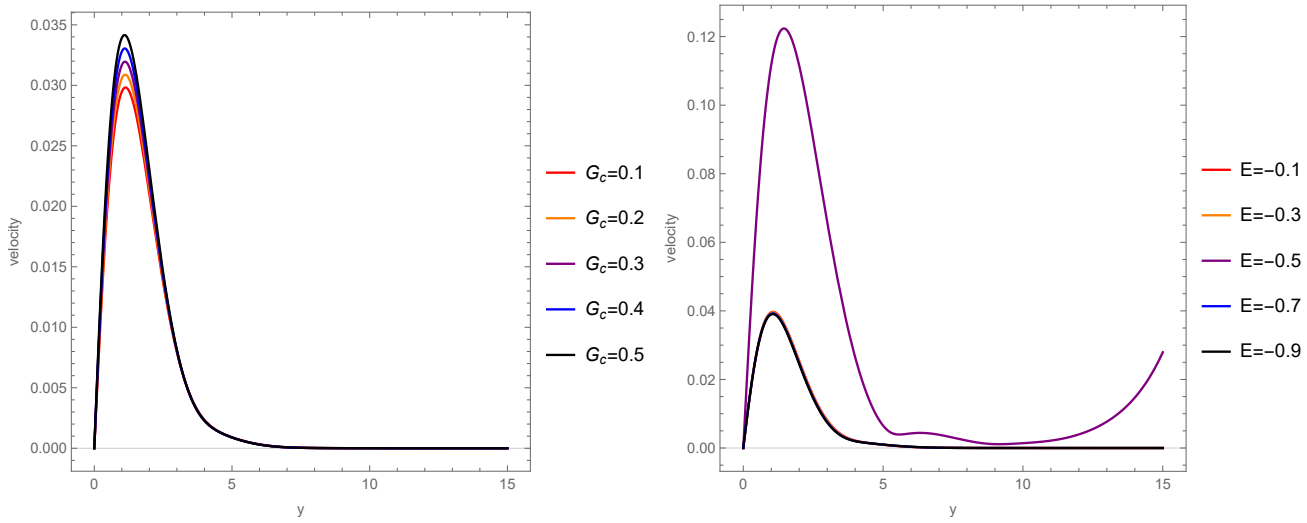

(c) Variation of $q(y,t)$ for (Grashof number for mass transfer G_c).

(d) Variation of $q(y,t)$ for (Rotation parameter E).

Figure 4: Variation of velocity with different flow parameters

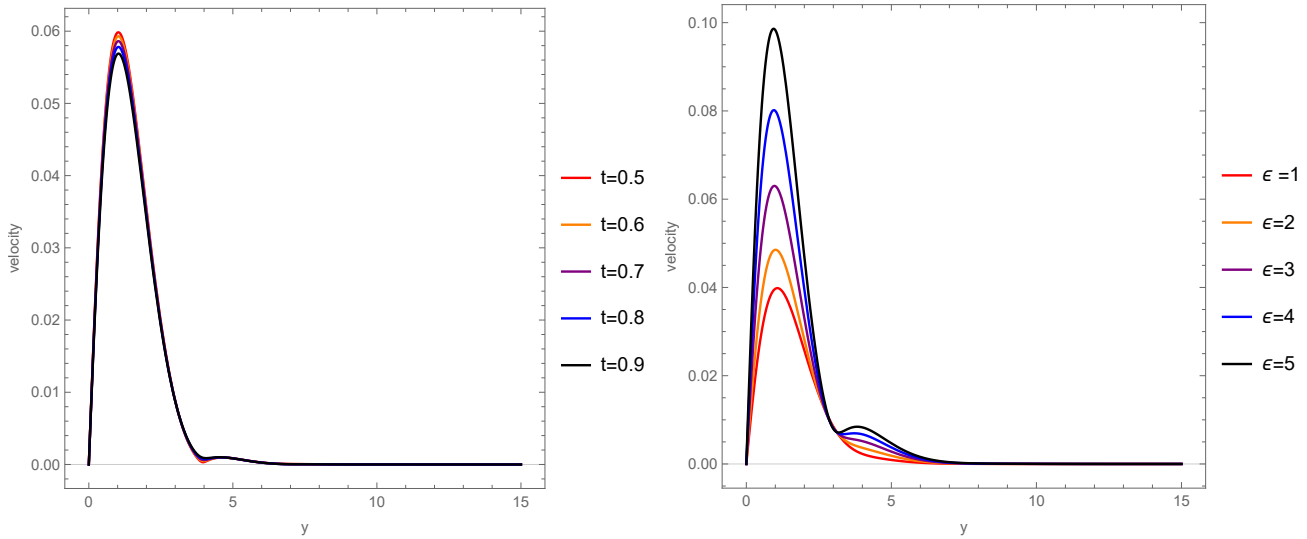

(a) Variation of $q(y,t)$ for (Time t).

(b) Variation of $q(y,t)$ for (A small positive constant ϵ).

Figure 5: Variation of velocity with different flow parameters

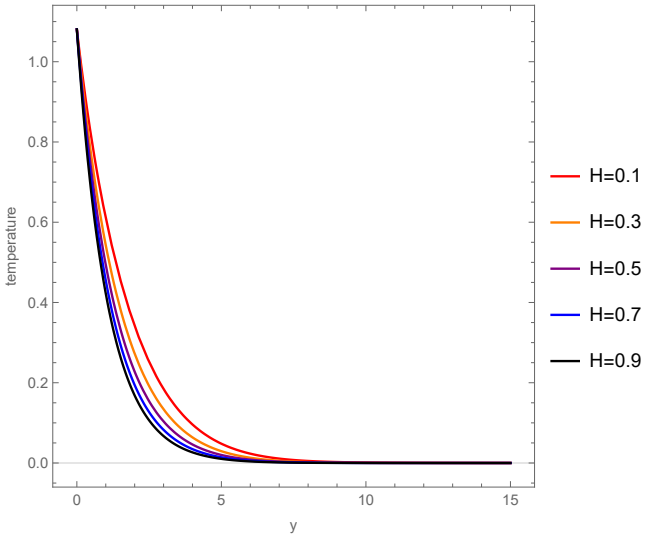

(a) Variation of $T(y,t)$ for (Heat Source parameter H).

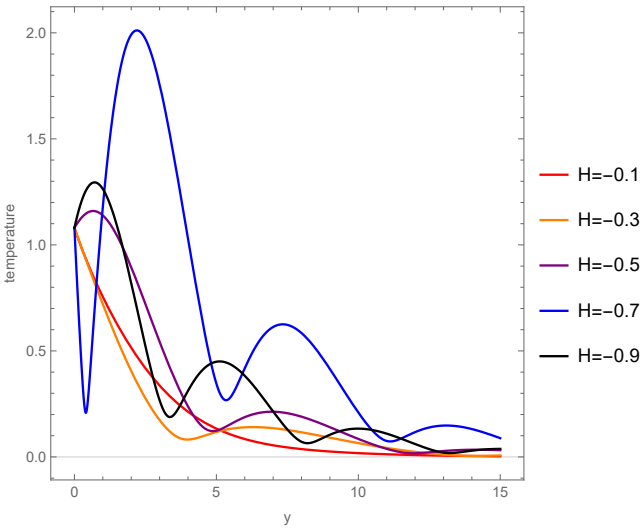

(b) Variation of $T(y,t)$ for (Heat Source parameter H).

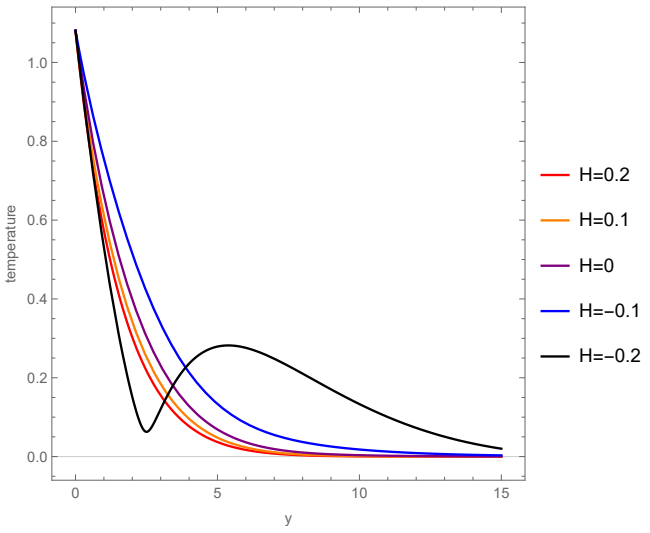

(c) Variation of $T(y,t)$ for (Heat Source parameter H).

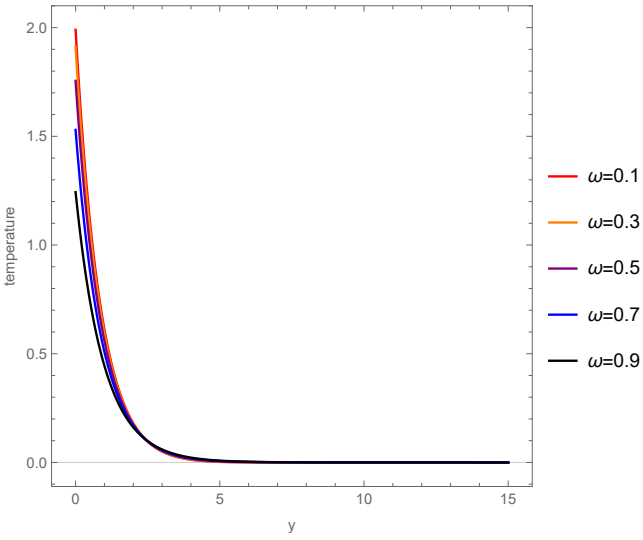

(d) Variation of $T(y,t)$ for (Frequency of oscillation ω).

Figure 6: Variation of temperature with different flow parameters

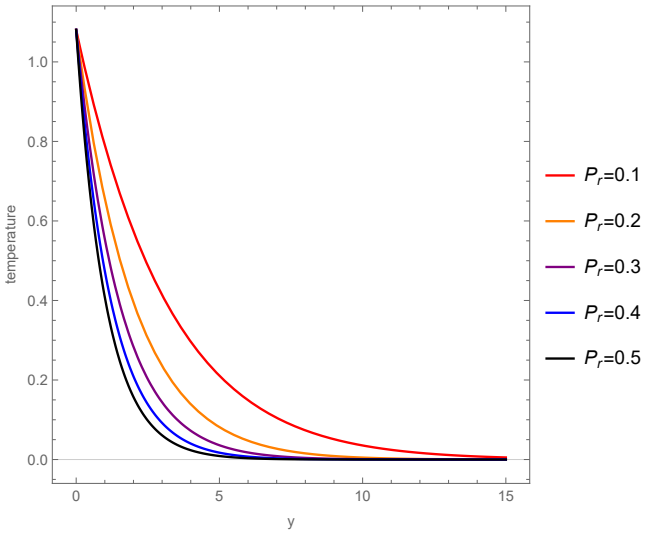

(a) Variation of $T(y,t)$ for (Prandtl number P_r).

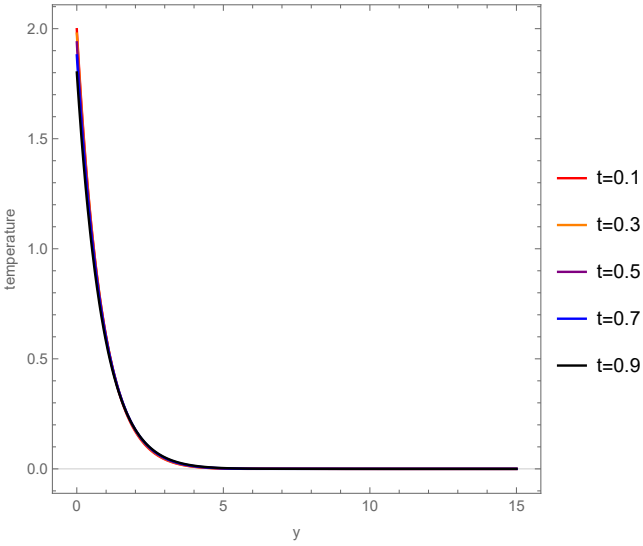

(b) Variation of $T(y,t)$ for (Time t).

Figure 7: Variation of temperature with different flow parameters

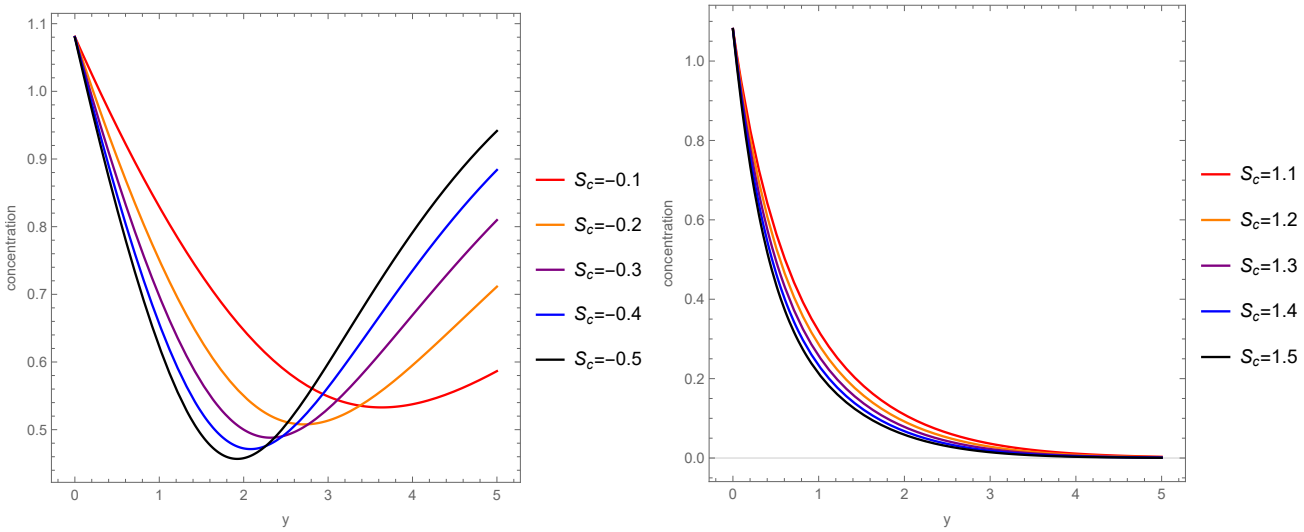

(a) Variation of $C(y,t)$ for (Schmidt number S_c).

(b) Variation of $C(y,t)$ for (Schmidt number S_c).

Figure 8: Variation of concentration with different flow parameters

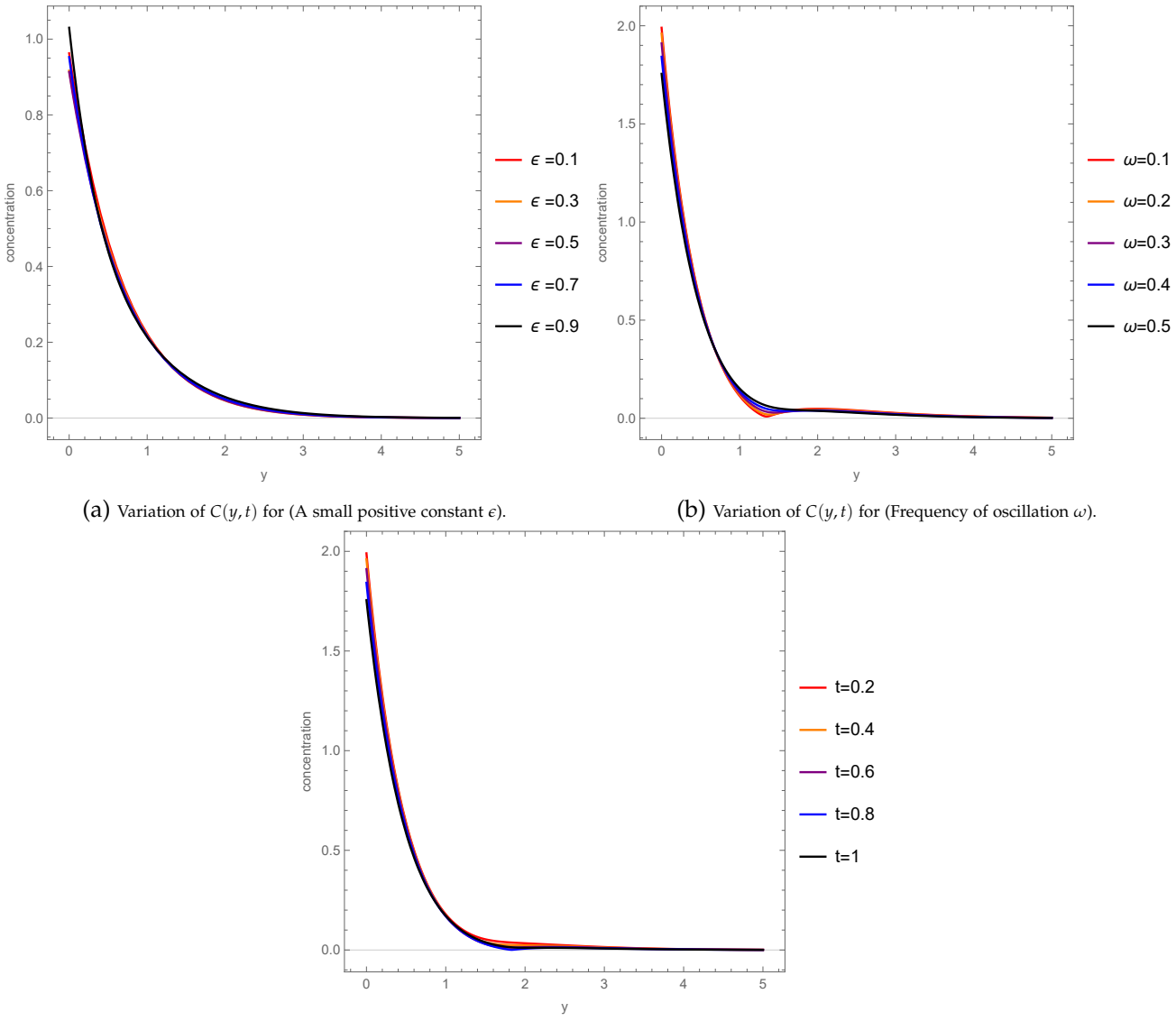

(a) Variation of $C(y,t)$ for (A small positive constant ϵ).

(b) Variation of $C(y,t)$ for (Frequency of oscillation ω).

(c) Variation of $C(y,t)$ for (Time t).

Figure 9: Variation of concentration with different flow parameters

ωt	$M=1$	$M=2$	$M=3$	$M=4$	$M=5$
0	0.204493	0.14301	0.104464	0.0808941	0.0653978
$\frac{\pi}{4}$	0.197003	0.13642	0.0991672	0.0765842	0.0617945
$\frac{\pi}{2}$	0.16543	0.113116	0.08168	0.0627797	0.0504482
$\frac{3\pi}{4}$	0.114091	0.0773117	0.0553295	0.0421402	0.0335354

Table 1: Variation in Share Stress at the Plate with Magnetic Parameter M at $\omega = 1$, $\phi = 2$, $K_p = 0.6$, $P_r = 0.5$, $G_c = 1$, $G_r = 1$, $S_c = 1.5$, $H = 1$, $\varepsilon = 1$, $t = 2$, $E = 0.5$.

ωt	$\phi=2$	$\phi=5$	$\phi=10$	$\phi=15$	$\phi=20$
0	0.104464	0.0653703	0.0447076	0.0354718	0.0299862
$\frac{\pi}{4}$	0.0991672	0.0623946	0.0428697	0.0341107	0.0288956
$\frac{\pi}{2}$	0.08168	0.0520465	0.0361385	0.028941	0.024631
$\frac{3\pi}{4}$	0.0553295	0.0364917	0.0260348	0.0211846	0.0182336

Table 2: Variation in Share Stress at the Plate with Couple Stress Parameter ϕ at $M = 3$, $\omega = 1$, $K_p = 0.6$, $P_r = 0.5$, $G_c = 1$, $G_r = 1$, $S_c = 1.5$, $H = 1$, $\varepsilon = 1$, $t = 2$, $E = 0.5$.

ωt	$K_p=0.1$	$K_p=0.2$	$K_p=0.3$	$K_p=0.4$	$K_p=0.5$
0	0.0895075	0.0982106	0.101363	0.102935	0.10386
$\frac{\pi}{4}$	0.0843637	0.0928814	0.0960224	0.0976071	0.0985485
$\frac{\pi}{2}$	0.0675583	0.0752542	0.0783269	0.0799688	0.0809874
$\frac{3\pi}{4}$	0.0414072	0.0480892	0.0512808	0.0531743	0.0544321

Table 3: Variation in Share Stress at the Plate with Porosity Parameter K_p at $M = 3$, $\omega = 1$, $\phi = 2$, $P_r = 0.5$, $G_c = 1$, $G_r = 1$, $S_c = 1.5$, $H = 1$, $\varepsilon = 1$, $t = 2$, $E = 0.5$.

ωt	$H = 0.1$	$H = 0.2$	$H = 0.3$	$H = 0.4$	$H = 0.5$
0	0.128811	0.124779	0.121197	0.118026	0.115197
$\frac{\pi}{4}$	0.123112	0.118687	0.115103	0.112036	0.109337
$\frac{\pi}{2}$	0.102258	0.098379	0.0952645	0.092626	0.0903186
$\frac{3\pi}{4}$	0.0709643	0.068003	0.0656227	0.0636088	0.0618523

Table 4: Variation in Share Stress at the Plate with Heat Source Parameter H at $M = 3$, $\omega = 1$, $\phi = 2$, $K_p = 0.6$, $G_c = 1$, $G_r = 1$, $P_r = 0.5$, $S_c = 1.5$, $\varepsilon = 1$, $t = 2$, $E = 0.5$.

ωt	$G_r = 0.1$	$G_r = 0.3$	$G_r = 0.5$	$G_r = 0.7$	$G_r = 0.9$
0	0.0380533	0.052811	0.0675689	0.082327	0.0970851
$\frac{\pi}{4}$	0.0370188	0.0508129	0.0646216	0.0784372	0.0922566
$\frac{\pi}{2}$	0.031934	0.0428685	0.0539068	0.064996	0.0761139
$\frac{3\pi}{4}$	0.024457	0.0310109	0.0378188	0.044765	0.0517939

Table 5: Variation in Share Stress at the Plate with Grashof number for heat transfer G_r at $M = 3$, $\omega = 1$, $\phi = 2$, $K_p = 0.6$, $P_r = 0.5$, $G_c = 1$, $S_c = 1.5$, $H = 1$, $\varepsilon = 1$, $t = 2$, $E = 0.5$.

ωt	$P_r = 0.1$	$P_r = 0.2$	$P_r = 0.3$	$P_r = 0.4$	$P_r = 0.5$
0	0.172513	0.146622	0.128751	0.115205	0.104464
$\frac{\pi}{4}$	0.162353	0.138364	0.121763	0.109165	0.0991672
$\frac{\pi}{2}$	0.130484	0.112109	0.0992664	0.089472	0.08168
$\frac{3\pi}{4}$	0.0814407	0.0718543	0.0649475	0.0596067	0.0553295

Table 6: Variation in Share Stress at the Plate with Prandtl number P_r at $M = 3$, $\omega = 1$, $\phi = 2$, $K_p = 0.6$, $G_c = 1$, $G_r = 1$, $S_c = 1.5$, $H = 1$, $\varepsilon = 1$, $t = 2$, $E = 0.5$.

ωt	$S_c = 1.3$	$S_c = 1.4$	$S_c = 1.5$	$S_c = 1.6$	$S_c = 1.7$
0	0.11177	0.107869	0.104464	0.101482	0.0988613
$\frac{\pi}{4}$	0.106399	0.102539	0.0991672	0.0962136	0.0936191
$\frac{\pi}{2}$	0.0877014	0.0844955	0.08168	0.0792018	0.0770156
$\frac{3\pi}{4}$	0.0593426	0.057212	0.0553295	0.0536623	0.0521822

Table 7: Variation in Shear Stress at the Plate with Schmidt number S_c at $M = 3$, $\omega = 1$, $\phi = 2$, $K_p = 0.6$, $P_r = 0.5$, $G_c = 1$, $G_r = 1$, $H = 1$, $\varepsilon = 1$, $t = 2$, $E = 0.5$.

ωt	$G_c = 0.1$	$G_c = 0.2$	$G_c = 0.3$	$G_c = 0.4$	$G_c = 0.5$
0	0.0768587	0.0799259	0.0829932	0.0860604	0.0891277
$\frac{\pi}{4}$	0.0721398	0.0751395	0.0781403	0.081142	0.0841446
$\frac{\pi}{2}$	0.0584779	0.0610297	0.0635899	0.0661575	0.0687317
$\frac{3\pi}{4}$	0.0380394	0.0398736	0.0417365	0.0436243	0.0455339

Table 8: Variation in Share Stress at the Plate with Grashof number for mass transfer G_c at $M = 3$, $\omega = 1$, $\phi = 2$, $K_p = 0.6$, $P_r = 0.5$, $G_r = 1$, $S_c = 1.5$, $H = 1$, $\varepsilon = 1$, $t = 2$, $E = 0.5$.

ωt	$E = -0.1$	$E = -0.3$	$E = -0.5$	$E = -0.7$	$E = -0.9$
0	0.104683	0.10461	0.104464	0.104248	0.103963
$\frac{\pi}{4}$	0.0993462	0.099266	0.0991169	0.098901	0.0986205
$\frac{\pi}{2}$	0.0818224	0.0817537	0.0816283	0.0814482	0.0812156
$\frac{3\pi}{4}$	0.0553728	0.0553095	0.055209	0.0550731	0.0549036

Table 9: Variation in Share Stress at the Plate with Rotation parameter E at $M = 3$, $\omega = 1$, $\phi = 2$, $K_p = 0.6$, $P_r = 0.5$, $G_c = 1$, $G_r = 1$, $S_c = 1.5$, $H = 1$, $\varepsilon = 1$, $t = 2$.

ωt	$P_r = 0.1$	$P_r = 0.2$	$P_r = 0.3$	$P_r = 0.4$	$P_r = 0.5$
0	0.798121	1.23834	1.6254	1.98695	2.33333
$\frac{\pi}{4}$	0.724465	1.12729	1.48263	1.81528	2.1345
$\frac{\pi}{2}$	0.517296	0.815131	1.08144	1.33304	1.57614
$\frac{3\pi}{4}$	0.22785	0.378379	0.519762	0.657655	0.794022

Table 10: Variation in Nusslet Number at the Plate with Prandtl Number P_r at $M = 3$, $\omega = 1$, $\phi = 2$, $K_p = 0.6$, $G_c = 1$, $G_r = 1$, $S_c = 1.5$, $H = 1$, $\varepsilon = 1$, $t = 2$, $E = 0.5$.

ωt	$H = 0.1$	$H = 0.2$	$H = 0.3$	$H = 0.4$	$H = 0.5$
0	1.60716	1.71127	1.80754	1.89668	1.97984
$\frac{\pi}{4}$	1.46	1.56267	1.65255	1.73437	1.81037
$\frac{\pi}{2}$	1.09824	1.16631	1.22772	1.28476	1.33859
$\frac{3\pi}{4}$	0.679905	0.681496	0.688298	0.698563	0.711292

Table 11: Variation in Nusslet Number at the Plate with Heat Source Parameter H at $M = 3$, $\omega = 1$, $\phi = 2$, $K_p = 0.6$, $P_r = 0.5$, $G_c = 1$, $G_r = 1$, $S_c = 1.5$, $\varepsilon = 1$, $t = 2$, $E = 0.5$.

ωt	$S_c = 0.1$	$S_c = 0.2$	$S_c = 0$	$S_c = -0.1$	$S_c = -0.11$
0	0.300044	0.746589	0.02	0.0000317835	0.0000146981
$\frac{\pi}{4}$	0.301629	0.548876	0.0184776	0.165486	0.172008
$\frac{\pi}{2}$	0.282423	0.623508	0.0141421	0.246871	0.257301
$\frac{3\pi}{4}$	0.283115	0.324475	0.00765367	0.309508	0.322967

Table 12: Variation in Sherwood Number at the Plate with Schmidt Number S_c at $M = 3$, $\omega = 1$, $\phi = 2$, $K_p = 0.6$, $P_r = 0.5$, $G_c = 1$, $G_r = 1$, $S_c = 1.5$, $H = 1$, $\varepsilon = 1$, $t = 2$, $E = 0.5$.

6. Conclusion

This study investigates the unsteady free convective heat and mass transfer flow of a couple-stress, incompressible, and electrically conducting fluid past a vertical non-homogeneous porous plate embedded in a porous medium. The analysis incorporates the effects of time-dependent oscillatory permeability, suction, a transverse magnetic field, rotation, and a heat source/sink. The governing equations are solved using a multi-parameter perturbation technique to obtain approximate analytical expressions for the velocity, temperature, and concentration distributions. Based on the graphical illustrations and numerical computations, the principal conclusions of the study are summarized as follows:

1. The velocity of the fluid is observed to decrease significantly with increasing values of the magnetic parameter M, couple-stress parameter ϕ, oscillation frequency ω, Prandtl number P_r, and Schmidt number S_c. This reduction in velocity can be attributed to the combined resistive effects arising from the Lorentz force generated by the applied magnetic field, the intensified internal resistance due to couple-stress characteristics of the fluid, the diminished thermal diffusivity associated with higher P_r, and the reduced mass diffusivity corresponding to elevated values of S_c.

2. The results indicate that increasing the thermal Grashof number (G_r) and the mass Grashof number (G_c) leads to a marked enhancement in the velocity distribution. This behavior underscores the significant contribution of thermal and solutal buoyancy forces in driving and accelerating the fluid flow.

3. The velocity profile exhibits an upward trend with increasing values of the porosity parameter (K_p) and the oscillatory suction parameter (ϵ), owing to the reduced flow resistance within the porous medium and the intensified suction effects at the plate.

4. The temperature distribution decreases with increasing Prandtl number (P_r) and oscillation frequency (ω), leading to a reduction in the thickness of the thermal boundary layer. This behavior can be attributed to diminished thermal diffusivity and the suppression of thermal diffusion at higher oscillation frequencies.

5. The heat source parameter (H) exerts a significant influence on the thermal field. Positive values of H result in a reduction in temperature and a thinner thermal boundary layer, whereas negative values enhance the temperature distribution and give rise to oscillatory thermal behavior.

6. The concentration profile decreases with an increase in the Schmidt number (S_c), indicating that greater resistance to mass diffusivity weakens species diffusion and consequently reduces the concentration boundary layer thickness.

7. The skin friction coefficient at the plate decreases with increasing magnetic parameter (M), couple-stress parameter (ϕ), Prandtl number (P_r), Schmidt number (S_c), and heat source parameter (H). Conversely, it increases with higher values of the permeability parameter (K_p), thermal Grashof number (G_r), and solutal Grashof number (G_c), owing to the enhancement of permeability and buoyancy forces.

8. The Nusselt number (N_u) increases with increasing Prandtl number (P_r) and heat source parameter (H), indicating improved heat transfer at the plate. However, for fixed parameter values, N_u decreases with an increase in the phase angle (ωt).

9. The Sherwood number (S_h) increases with increasing Schmidt number (S_c) and phase angle, reflecting enhanced mass transfer rates at the plate due to stronger diffusivity effects.

10. In summary, the combined effects of the magnetic field, rotational dynamics, thermal influences, and mass diffusion mechanisms provide an effective means of controlling heat and mass transfer characteristics in couple-stress fluid flow through a porous medium under oscillatory conditions.

7. Acknowledgment

The author acknowledge this work is part of the research program for the award of Ph.D. degree to the first author. The authors express their gratitude to the learned reviewers for their valuable comments and suggestions which improved the present work to a great extent.

References

[1] S. S. Das, A. Satapathy, J. K. Das and J. P. Panda, *Mass transfer effects on MHD flow and heat transfer past a vertical porous plate through a porous medium under oscillatory suction and heat source*, International Journal of Heat and Mass Transfer, 52(25-26)(2009), 5962-5969.

[2] P. Dash, K. L. Ojha, B. K. Swain and G. C. Dash, *MHD Couette flow and heat transfer in a rotating channel in presence of viscous dissipation and heat source/sink*, Numerical Heat Transfer, Part A: Applications, 85(20)(2011), 3472-3487.

[3] J. G. Kumar and P. V. Satyanarayana, *Mass transfer effects on MHD unsteady free convective Walter's memory flow with constant suction and heat sink*, International Journal of Applied Mathematics and Mechanics, 7(19)(2011), 97-109.

[4] O. Prakash, D. Kumar and Y. K. Dwivedi, *Heat transfer in MHD flow of dusty viscoelastic (Walters' liquid model–B) stratified fluid in a porous medium under variable viscosity*, Pramana, 79(6)(2012), 1457-1470.

[5] V. Ravikumar, M. C. Raju and G. S. S. Raju, *Heat and mass transfer effects on MHD flow of viscous fluid through non-homogeneous porous medium in presence of temperature dependent heat source*, International Journal of Contemporary Mathematical Sciences, 7(32)(2012), 1597-1604.

[6] S. A. Hussaini, M. V. Ramana Murthy and A. Waheedullah, *MHD unsteady memory convective flow through porous medium with variable suction*, Journal of Applied Fluid Mechanics, (2013).

[7] S. R. Mishra, G. C. Dash and M. Acharya, *Mass and heat transfer effect on MHD flow of a visco-elastic fluid through porous medium with oscillatory suction and heat source*, International Journal of Heat and Mass Transfer, 57(2)(2013), 433-438.

[8] B. Mohanty, S. R. Mishra and H. B. Pattnaik, *MHD flow of a viscoelastic fluid through non-homogeneous porous medium with oscillatory suction and heat source/sink*, International Journal of Mathematics Education, 4(2014), 21-34.

[9] D. Srinivasacharya and K. Kaladhar, *Mixed convection in a couple stress fluid with Soret and Dufour effects*, International Journal of Applied Mathematics and Mechanics, 7(20)(2011), 59-71.

[10] D. Srinivasacharya and K. Kaladhar, *Soret and Dufour effects on mixed convection flow of couple stress fluid in a non-Darcy porous medium with heat and mass fluxes*, Journal of Porous Media, 17(2)(2014).

[11] P. R. Sharma, Pooja Sharma and Ruchi Saboo, *MHD free convection radiative flow of visco-elastic fluid (Walter's liquid model–B) in the presence of chemical reaction*, Acta Technica, 60(2015), 359-373.

[12] Udayagiri, *Unsteady MHD free convection flow characteristics of a viscoelastic fluid past a vertical porous plate*, International Journal of Applied Science and Engineering, 14(2)(2016), 69-85.

[13] P. Ramaiah, V. S. Vijaya Kumar, K. Rama Krishna Prasad and K. S. Balamurugan, *Chemical reaction and radiation absorption effects on MHD convective heat and mass transfer flow of a viscoelastic fluid past an oscillating porous plate with heat generation/absorption*, International Journal of Chemical Sciences, 14(2)(2016), 548-570.

[14] P. D. Reddy, *Unsteady MHD free convection flow of a viscoelastic fluid past a vertical porous plate*, International Journal of Dynamics of Fluid, 13(1)(2017), 61-77.

[15] T. Suneetha and A. Sailakumari, *Heat and mass transfer characteristics of MHD free convective Rivlin–Ericksen fluid flow past a porous plate*, International Journal of Mathematics Trends and Technology, 53(2018).

[16] M. V. Krishna and A. J. Chamkha, *MHD peristaltic rotating flow of a couple stress fluid through a porous medium with wall and slip effects*, Special Topics & Reviews in Porous Media, 10(3)(2019).

[17] M. V. Krishna and K. Jyothi, *Heat and mass transfer on MHD rotating flow of a visco-elastic fluid through a porous medium with time-dependent oscillatory permeability*, The Journal of Analysis, 27(2)(2019), 643-662.

[18] K. V. B. Rajakumar, T. Govinda Rao, M. Umasankara Reddy and K. S. Balamurugan, *Influence of Dufour and thermal radiation on unsteady MHD Walter's liquid model–B flow past an impulsively started infinite vertical plate embedded in a porous medium with chemical reaction, Hall and ion slip current*, SN Applied Sciences, 2(4)(2020), 742.

[19] S. Poddar, M. M. Islam, J. Ferdouse and M. M. Alam, *Steady-state solution of MHD heat and mass transfer fluid flow over a semi-infinite vertical plate in a rotating system dipped in a porous medium*, International Journal of Heat & Technology, 40(2)(2022).

[20] M. Naveed, M. Imran and S. Gul, *Heat transfer analysis in hydromagnetic flow of couple stress fluid*, Advances in Mechanical Engineering, 15(2)(2023).

[21] A. Panya, *MHD Darcy-Forchheimer slip flow in a porous medium with variable thermo-physical properties*, Zenodo (CERN), (2023).

[22] I. W. A. Okuyade and T. M. Abbey, *Transient MHD fluid flow past a moving vertical surface in a velocity slip flow regime*, WSEAS Transactions on Fluid Mechanics, 19(2024), 99-112.

[23] M. K. Mishra and D. Kumar, *An analytical study of two-fluid flow in a porous inclined channel*, Global Journal of Pure and Applied Mathematics, 21(3)(2025), 565-583.

[24] S. Ahmad, *A time-fractional model of hydromagnetic slip flow*, Scientific Reports, 15(1)(2025).

[25] R. Pegu, D. Dey and D. Choudhury, *Numerical investigation on viscoelastic fluid flow*, International Communications in Heat and Mass Transfer, 168(2025).